Eur Biophys J (1998) 27: 43–53 © Springer-Verlag 1998

ARTICLE

S. Kakorin · E. Redeker · E. Neumann

Electroporative deformation of salt filled lipid vesicles

Received: 8 July 1997 / Accepted: 15 September 1997

Abstract Membrane electroporation, vesicle shape deformation and aggregation of small, NaCl-filled lipid vesicles (of radius a = 50 nm) in DC electric fields was characterized using conductometric and turbidimetrical data. At pulse durations $t_E \leq 55 \pm 5$ ms the increase in the conductivity of the vesicle suspension is due to the field-induced efflux of electrolyte through membrane electropores. Membrane electroporation and Maxwell stress on the vesicle membrane lead to vesicle elongation concomitant with small volume reduction (up to 0.6% in an electric field of E = 1 MV m^{-1}). At $t_E > 55 \pm 5$ ms, further increases in the conductivity and the optical density suggest electroaggregation and electrofusion of vesicles. The conductivity changes after the electric pulse termination reflect salt ion efflux through slowly resealing electropores. The analysis of the volume reduction kinetics yields the bending rigidity $\kappa = (4.1 \pm 0.3) \cdot 10^{-20}$ J of the vesicle membrane. If the flow of Na^+ and Cl^- ions from the vesicle interior is treated in terms of Hagen-Poiseuille's equation, the number of permeable electropores is N = 39 per vesicle with mean pore radius $r_p = 0.85 \pm 0.05$ nm at E = 1 MVm^{-1} and $t_E \leq 55 \pm 5$ ms. The turbidimetric and conductometric data suggest that *small* lipid vesicles ($a \leq 50$ nm) are not associated with extensive membrane thermal undulations or superstructures. In particular with respect to membrane curvature, the vesicle results are suggestive for the design and optimization of electroporative delivery of drugs and genes to cell tissue at small field strengths (≤ 1 MVm^{-1}) and large pulse durations (≤ 100 ms).

Key words Vesicle electroaggregation and electrofusion · Electroporative conductometry and turbidimetry

S. Kakorin · E. Redeker · E. Neumann (✉)
Physical and Biophysical Chemistry, Faculty of Chemistry, University of Bielefeld, P. O. Box 100 131, D-33501 Bielefeld, Germany
(e-mail: eberhard.neumann@post.uni-bielefeld.de)

Abbreviations a Vesicle radius · γ Reduced distance between the vesicle centers; $\gamma = h/a \cdot \gamma_0$ Average reduced distance between the vesicle centers; $\gamma_0 = h_0/a$ at E = 0 · γ_p Pore partition coefficient; $\gamma_p = [n^p]/[n^{in}] \cdot \gamma_m$ Conventional membrane partition coefficient · D Diffusion coefficient of ions passing electropores · E External electrical field strength · f_p Fraction of porated membrane surface · $\Delta\varphi_{th}$ Threshold value of the transmembrane potential drop · H Vesicle membrane curvature; $H = 1/a \cdot h$ Distance between the centers of two approaching vesicles · h_0 Average distance between the centers of two vesicles at E = 0 · κ Membrane bending rigidity · $\lambda_T(t)$ Suspension conductivity after application of an electric pulse (at time t) · $\lambda_L(t)$ Suspension conductivity without application of an electric pulse due to salt leakage · $\lambda_R(t)$ Conductivity of the blank solution of sucrose and NaCl due to Joule heating · λ_0 Initial conductivity of vesicle suspension before pulse application · $\Delta\lambda^I$ Amplitude value of the phase I at time $t = t_E$ · $\Delta\lambda^{II}$ Amplitude value of the phase II at $t \rightarrow \infty$ · λ_{max} Maximum conductivity due to salt released from vesicles in the bathing solution · λ_{in} Conductivity of electrolyte in the vesicle interior · λ_{max} Membrane conductivity · λ_{ves} Total conductivity of a vesicle (i.e. vesicle membrane and vesicle interior) · λ_{ex} Conductivity of the extravesicular medium · $[n^p]$ Molar concentration of ions in the pore water · $[n^{in}]$ Molar concentration of ions within the vesicle · n^{in} Amount of electrolyte in the intravesicular medium · n_0^{in} Amount of electrolyte in the vesicle at the end of the pulse · n^{out} Amount of electrolyte in the extravesicular bulk medium · N Number of membrane pores per vesicle (N^0, maximum number) · ζ Increase of vesicle radius in the direction of the maximal elongation · ξ Maximum conductivity factor (λ_{max}/λ_0) · P_p Pore permeability coefficient · P_m Conventional membrane permeability coefficient · r_p Mean pore radius · S_p Total area of pore surfaces ($S_p = N \cdot \pi \cdot r^2$) · S_p^0 Maximum total area of pore surfaces ($S_p^0 = N^0 \cdot \pi \cdot r^2$) · t_E Pulse duration · V^{in} Volume of intravesicular medium · V^{out} Volume of extravesicular medium

Introduction

Membrane electroporation and shape deformation of lipid vesicles in an electric field have frequently been the subject of both advanced experimental techniques (Kummrow and Helfrich 1991; Neumann et al. 1992; Kinosita et al. 1992; Hibino et al. 1993) and sophisticated mathematical theories (Winterhalter and Helfrich 1988; Neumann 1989; Hyuga et al. 1993; Sokirko et al. 1994; Seifert 1995; Kakorin et al. 1996). Membrane electroporation (ME) is an electrical technique to render lipid membranes porous and permeable, transiently and reversibly, by external voltage pulses. Recently, ME has gained increasing importance in cell biology, biotechnology (Neumann and Kakorin 1996) and medicine, in particular in the new field of electroporative chemotherapy; see, e.g., Heller et al. (1996). The "electro-deformation" of lipid vesicles is possibly a mechanism to provide larger pores leading to transmembrane transport or causing membrane rupture. Proper analysis of vesicle deformation yields the elastic rigidity of the membrane (Kummrow and Helfrich 1991).

There are some theoretical estimates of the deformation kinetics of small vesicles (Sokirko et al. 1994). Electrodeformation of giant vesicles can be easily observed in the light microscope. The enormous increase in membrane area (≥15%) was suggested to be due to an optically invisible superstructure or membrane roughness (Kummrow and Helfrich 1991). In contrast to giant vesicles, cryotransmission electron-micrographs of small vesicles of radius $20 \le a/\mathrm{nm} \le 200$ show rather smooth surfaces as compared to the flaccid giant vesicles depicted on the same scale (Klösgen and Helfrich 1993). Apparently, the large membrane curvature of the small vesicles is incompatible with superstructure.

Another membrane area reservoir available for vesicle deformation is the thermal membrane undulations superimposed on an average, equilibrium vesicle shape (Helfrich and Servus 1984; Seifert 1996). However, the small lateral membrane tension ($\sigma \approx 1\ \mathrm{mN\ m^{-1}}$) inherent to all lipid bilayers in water should render the thermal undulations of membranes negligibly small (Steiner and Adam 1984).

Our approach to investigate ME and shape deformation of small vesicles (which are invisible in the light microscope) is to load the vesicles with highly concentrated electrolyte and to measure the kinetics of the conductivity increase caused by an electric pulse. The optical density of the vesicle suspension yields additional information concerning vesicle shape deformation, electroaggregation and electrofusion. The data permit one to specify the mechanism of vesicle deformation in an electric field; for instance, to decide whether the deformation is due to a membrane superstructure or thermal membrane undulations or whether the ion efflux from the vesicle interior is caused by (a few) membrane electropores. The analysis of the conductometric and optical data provides the rate constant of vesicle deformation, the membrane bending rigidity, mean pore size and estimates of pore numbers per vesicle.

Materials and methods

Preparation of salt-filled lipid vesicles

Unilamellar vesicles of a very homogeneous size distribution were prepared from phosphatidylcholine (PC) and Na-phosphatidylglycerol (PG), from Lipoid KG by the extruder technique (Hope et al. 1985; MacDonald et al. 1991). A homogenized mixture of 50% PC and 50% PG (w/w) was suspended in 0.5 M NaCl solution and freeze-thawed five times in liquid nitrogen to obtain solute equilibrium between trapped and bulk solution. With the LiposoFast mini-extruder the multilamellar vesicles were extruded 21 times through two stacked polycarbonate filters of nominal pore size 100 nm (Avestin) to produce 100 ± 5 nm vesicles (Mayer et al. 1996). In order to remove external NaCl, the vesicle suspension was dialyzed against sucrose solution of the same osmolarity (0.7 M sucrose). The vesicle suspension was diluted with degassed sucrose solution to prepare aliquots of a final lipid concentration of 1 mM.

Electroporation protocol and conductivity measurements

Rectangular electric pulses were delivered with an Elektroporator (Dialog II, Düsseldorf). The field strengths E were increased up to $1\ \mathrm{MVm^{-1}}$ (at electrode distance 1 mm) and variable pulse lengths from $0.005 \le t_E/\mathrm{s} \le 1$. The sample cells were disposable spectrophotometer cuvettes with inserted stainless steel electrodes; they were thermostated at 293 K (20 °C). After the application of a single pulse, the suspension conductivity $\lambda_T(t)$ (Fig. 1 a, b) was measured with a KNICK digital conductometer (Krüss, Hamburg); response time constant <0.5 s. The time dependence $\lambda_L(t)$, without external field, is caused by leakage of salt ions through the vesicle membrane. In order to account for the conductivity changes due to Joule heating and electrode effects, the conductivity $\lambda_R(t)$ of the blank solution of sucrose and NaCl of identical initial conductivity as for the vesicle suspension was recorded after applying the same electrical pulse parameters. The relative change in suspension conductivity $\Delta\lambda(t)/\lambda_0$ is therefore solely due to salt efflux through the electropores and is given by:

$$\frac{\Delta\lambda(t)}{\lambda_0} = \frac{\left(\Delta\lambda_T(t) - \Delta\lambda_R(t) - \Delta\lambda_L(t)\right)}{\lambda_0} \qquad (1)$$

where λ_0 is in the initial suspension conductivity before pulse application; typically $\lambda_0 = \lambda_T(0) = 0.58\ \mathrm{mS/m}$, and $\Delta\lambda_T(t) = \lambda_T(t) - \lambda_0$, $\Delta\lambda_R(t) - \lambda_0$, $\Delta\lambda_L(t) - \lambda_0$.

Optical density measurements

The optical density OD or turbidity of the vesicle suspension was measured at a wavelength of $\lambda = 300$ nm with a KONTRON 860 spectrometer with thermostat control (re-

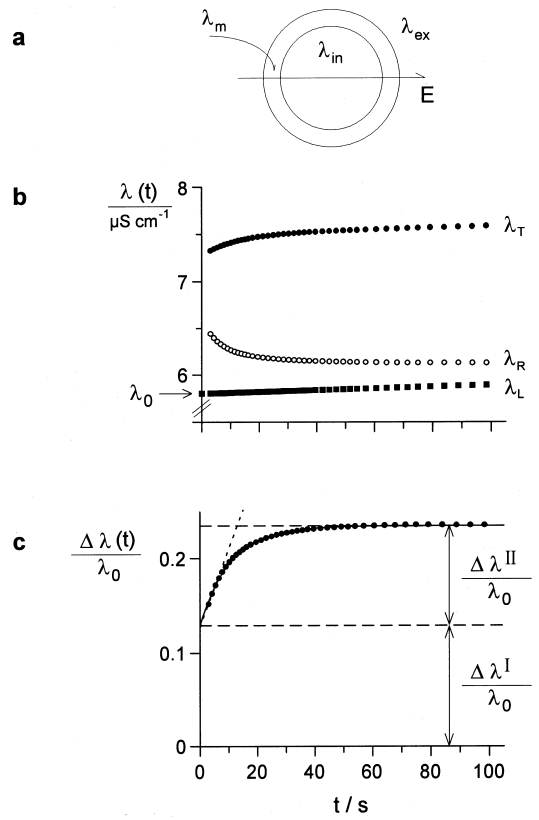

Fig. 1 **a** Cross section of a salt-filled vesicle in an electric DC field E; λ_m, λ_{in} and λ_{ex} are the conductivities of the vesicle membrane, vesicle interior (electrolyte) and external medium (sucrose solution), respectively. **b** The total conductivity $\lambda_T(t)$ of a suspension of salt-filled lipid vesicles and the reference conductivity $\lambda_R(t)$ of the blank solution, both treated with one rectangular electric pulse, as a function of post-field time t at E = 1 MVm^{-1} and t_E = 70 ms. Vesicles from PG and PC in the molar ratio of 1:1 at total lipid concentration 1 mM and radius a = 50 nm, filled with 0.5 M NaCl, are suspended in 0.7 M sucrose solution: λ_0 = 0.58 mSm^{-1}, T = 293 K; $\lambda_L(t)$ is due to leakage of salt through the vesicle membrane. The nominal concentrations of NaCl (=1.0 M in ions) in the vesicle interior and 0.7 M of sucrose, resulting in equal thermodynamic activities a(NaCl) = a(sucrose), were chosen to reduce the osmotic gradient to zero according to the standard procedure. **c** The relative conductivity change $\Delta\lambda(t)/\lambda_0 = (\Delta\lambda_T(t) - \Delta\lambda_R(t) - \Delta\lambda_L(t))/\lambda_0$. The data suggest the existence of at least two different phases: phase I (not time-resolved) includes all changes in conductance at the end of the pulse and is characterized by the value $\Delta\lambda^I(t)/\lambda_0$, determined by extrapolation of $\Delta\lambda(t)/\lambda_0$ to t = 0 corresponding to the end of the pulse at t_E. The amplitude of the time-resolved phase II is defined by $\Delta\lambda^{II}/\lambda_0 = (\Delta\lambda(t \to \infty) - \Delta\lambda^I(t))/\lambda_0$

sponse time constant <0.5 s). The same cuvette was used for the electroporation experiment. The data analysis uses the relative change in the OD of the suspension defined as:

$$\frac{\Delta OD}{OD_0} = \frac{OD_E - OD_0}{OD_0} \qquad (2)$$

where OD_0 and OD_E are the stationary values of the optical densities before the treatment with the electric field pulse and 10 min after the pulse application, respectively, where there was no further change in OD.

Results

The relative change in the suspension conductivity $\Delta\lambda(t)/\lambda_0$ of the salt-filled lipid vesicles after an electric field pulse (Fig. 1c) is characterized by at least two kinetic phases: a rapid phase I, not time-resolved is probably solely the result of the pulse (up to 100 ms). The slow phase II of the post-field time interval has a characteristic time constant of $\tau \approx 15$ s.

The amplitude $\Delta\lambda^I/\lambda_0$ of the phase I was determined by extrapolating the measured conductivity changes

$$\Delta\lambda(t)/\lambda_0 = \left(\Delta\lambda^I(t_E) + \Delta\lambda^{II}(t)\right)/\lambda_0 \qquad (3)$$

to the time point t = 0, corresponding to the end of pulse (t_E): $\Delta\lambda^I(t_E)/\lambda_0 = \Delta\lambda(t = 0)/\lambda_0$; $\Delta\lambda^{II}(t)/\lambda_0$ is the relative conductivity change of the second phase. The amplitude of phase II is defined by the difference:

$$\Delta\lambda^{II}/\lambda_0 = \left(\Delta\lambda(t \to \infty) - \Delta\lambda^I\right)/\lambda_0 \qquad (4)$$

A common feature of both phases is that they exhibit intermediate plateaus as a function of the pulse duration t_E (Fig. 2a, b). After the end of the plateau at $t_E \approx 55$ ms further, steep increases in both $\Delta\lambda^I(t_E)/\lambda_0$ and $\Delta\lambda^{II}(t_E)/\lambda_0$ are observed.

At short pulse durations $t_E \leq 55 \pm 5$ ms, the amplitudes $\Delta\lambda^I(t_E)/\lambda_0$ as a function of E are practically independent of t_E (Fig. 3a). At longer pulse durations $t_E > 55 \pm 5$ ms, the increase in $\Delta\lambda^I(t_E)/\lambda_0$ with E is steeper with increasing t_E (Fig. 3b). As with phase I, the field dependence of the amplitude $\Delta\lambda^{II}(t_E)/\lambda_0$ of phase II at $t_E \leq 55$ ms is prac-

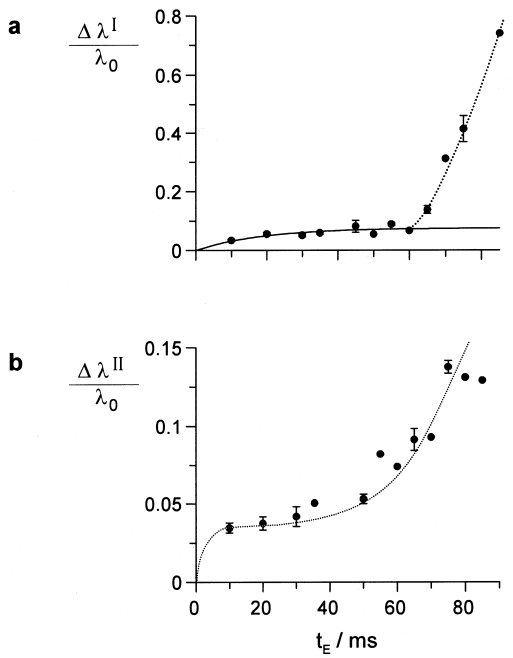

Fig. 2 The relative conductivity changes (**a**) $\Delta\lambda^I/\lambda_0$, and (**b**) $\Delta\lambda^{II}/\lambda_0$, as a function of the pulse duration t_E at E = 1 MVm^{-1}. The solid line in (**a**) corresponds to the calculation with Eq. (7) and Eq. (8) with $\kappa = (4.1 \pm 0.3) \cdot 10^{-20}$ J. Experimental conditions as in Fig. 1

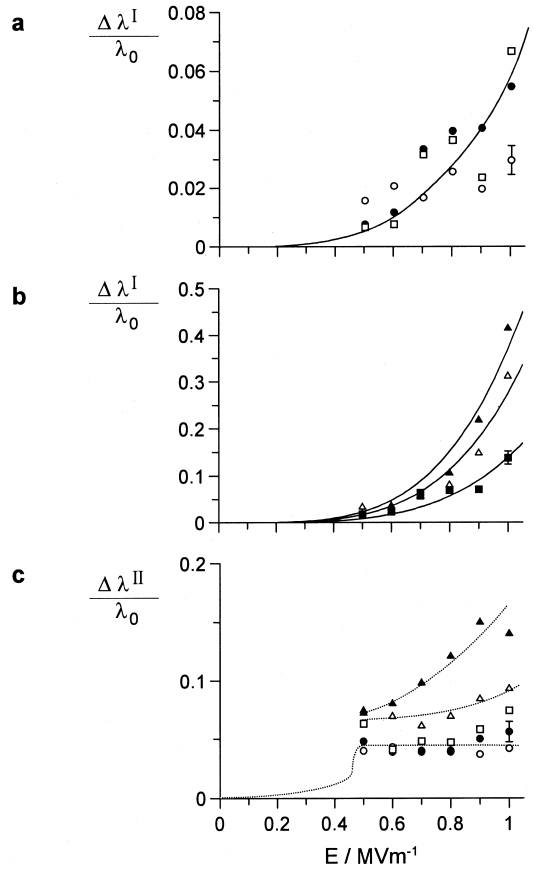

Fig. 3 Field strength dependencies of the conductivity phases I ($\Delta\lambda^I/\lambda_0$) at **a**: t_E/ms = 30 (○), 50 (●), 60 (□) and (b): t_E/ms = 65 (■), 70 (△), 75 (▲). The solid lines correspond to the calculations with Eq. (7) and Eq. (10). The bending rigidity $\kappa = (4.1 \pm 0.3) \cdot 10^{-20}$ J corresponds to the mean vesicle radius a = 50 nm at (a): t_E/ms = 30, 50, 60, and **b**: a/nm = 55, 65, 68 at t_E/ms = 65, 70, 75, respectively. **c**: field dependence of conductivity phases II ($\Delta\lambda^{II}/\lambda_0$) at: t_E/ms = 30 (○), 50 (●), 60 (□), 70 (△), 75 (▲) ms. Experimental conditions as in Fig. 1

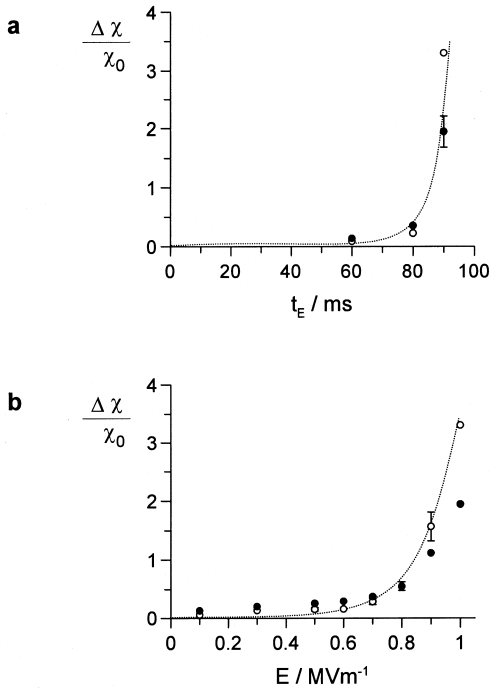

Fig. 4 Relative signal change $\Delta\chi/\chi_0$, (○) $\Delta OD/OD_0$ and (●) $\Delta\lambda/\lambda_0$, **a**: as a function of the pulse duration t_E at E = 1 MV m^{-1} and **b**: as a function of the field strength E at t_E = 90 ms. Experimental conditions as in Fig. 1

tically independent of the pulse duration; but at $t_E > 55$ ms they increase with t_E (Fig. 3c).

Parallel to $\Delta\lambda(t_E)/\lambda_0 = (\Delta\lambda^I(t_E) + \Delta\lambda^{II}(t_E))/\lambda_0$, the relative optical density $\Delta OD(t_E)/OD_0$ of the vesicle suspension increases very steeply after $t_E = 55 \pm 5$ at E = 1 MV m^{-1} (Fig. 4a). At constant pulse duration t_E = 90 ms, $\Delta\lambda(E)/\lambda_0$ and $\Delta OD(E)/OD_0$ both increase in parallel at $E \geq 0.9 \pm 0.1$ MV m^{-1} (Fig. 4b). Apparently, the two conductivity phases originate from different processes triggered by the field; they are, therefore, analyzed separately.

Data analysis and theory

ME triggers changes in the conductivity of vesicle suspensions

The electric field-induced increase in the suspension conductivity will be shown to originate from membrane electroporation. Actually, only membrane electropores can increase the ion transport through the membrane to a such a large extent. The field-induced change in the suspension conductivity is 10 to 100-fold larger than that due to the zero-field leakage of electrolyte from the lipid vesicles (Fig. 1b).

Conductivity phase I

The conductivity phase I may be related to the conductivity change during the field pulse ($t_E \leq 100$ ms). The intermediate plateau of $\Delta\lambda^I(t_E)$ (Fig. 2a) cannot be rationalized in terms of simple diffusive or electrodiffusive ion efflux through the electroporated membrane, which would be characterized by a monotone increase in $\Delta\lambda^I(t_E)$ with t_E. Both $\Delta\lambda^I(t_E)/\lambda_0$ and the plateau can, however, be consistently described by membrane electroporation and vesicle deformation. Actually $\Delta\lambda^I(t_E)/\lambda_0$ is due to the ion flow through the membrane electropores driven by the additional hydrostatic pressure produced by the Maxwell stress in the vesicle interior. The electric forces acting on the vesicle membrane result in a shape deformation of the vesicle. The efflux of ions from the vesicle to bulk solution occurs until the curvature-elastic forces opposing the Maxwell stress electric forces on the vesicle membrane are balanced. The steady-state amplitude of the deformation, corresponding to the balance of the electric and curvature-elastic forces, depends only on the electric field strength and the membrane bending rigidity, and not on the pulse

duration, provided that the elastic properties of the membrane remain unchanged during the pulse. In fact, if the membrane of a small vesicle is considered as practically unstretchable (neither thermal undulations nor membrane superstructure) the vesicle elongation in the field direction should lead to a reduction of the vesicle volume (Winterhalter and Helfrich 1988). Thus, the transition from a spherical vesicle to a spheroidal one is accompanied by an escape of internal solution from the vesicle interior. If the membrane permeability to water and ions due to electroporation is large enough, a steady state of the vesicle deformation can be reached in a time which is shorter than the pulse duration. In our case (Fig. 2a) the intermediate steady state or the plateau of $\Delta\lambda^I(t_E)/\lambda_0$ is reached with a time constant of 15 ± 2 ms.

The total amount of electrolyte leaving the vesicle interior depends on the vesicle elongation. For a small ellipsoidal elongation, $\zeta \ll a$, the vesicle volume reduction can be approximated by:

$$\Delta V = \frac{4}{3}\pi \cdot \left|(a+\zeta)(a-\zeta/2)^2 - a^3\right| \approx \pi \cdot a \cdot \zeta^2 \tag{5}$$

where ζ is the increase in the vesicle radius from a to a + ζ in the direction of the maximal elongation and $\zeta/2$ is the corresponding radius decrease in the orthogonal direction.

At low electrolyte concentration where the conductivity change is directly proportional to the amount of electrolyte which has escaped from the vesicle interior, we obtain for the relative conductivity change:

$$\frac{\Delta\lambda}{\lambda_{max}} = \frac{\Delta V}{V_0} \tag{6}$$

where λ_{max} is the maximum conductivity of the electrolyte, which would be reached if the salt is completely released from the vesicle interior into the solution and $V_0 = (4/3) \cdot \pi \cdot a^3$ is the initial volume of the vesicle.

The total content of NaCl entrapped in vesicles, determined by atom absorption spectrometry, is [NaCl] = 635 ± 2 μM and the corresponding conductivity of the salt in the bathing solution is λ_{max} = 3.91 ± 0.01 mS m^{-1}. As λ_0 = 0.58 ± 0.01 mS m^{-1}, the relative change of the conductivity $\Delta\lambda/\lambda_0$ (Eq. (1)) can be related to the relative vesicle volume change (Eq. (6)) according to:

$$\frac{\Delta\lambda}{\lambda_0} = \frac{\Delta\lambda}{\lambda_{max}} \cdot \frac{\lambda_{max}}{\lambda_0} = \xi \cdot \frac{\Delta V}{V_0} \tag{7}$$

where $\xi = \lambda_{max}/\lambda_0$.

Integration of the Hagen-Poiseuille equation for the volume flow from the vesicle interior (Eq. (A1) of appendix) yields:

$$\Delta V(t) \approx \Delta V_0 \cdot \left(1 - \exp(-t/\tau)\right) \tag{8}$$

where the volume relaxation rate is

$$\tau^{-1} = (96/5) \cdot N \cdot r_p^4 \cdot \kappa^2 / \left(d \cdot \eta \cdot a^9 \cdot \varepsilon_0 \cdot \varepsilon_w \cdot \left\{1 + a \cdot \lambda_m/(\lambda_{ex} \cdot d)\right\} \cdot E^2\right) \tag{9}$$

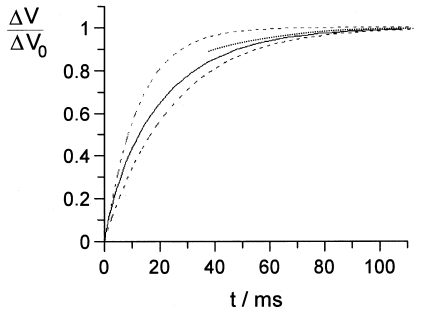

Fig. 5 Relative vesicle volume change in an electric field as a function of time, calculated according to the strict Eq. (A1) (solid curve), approximated with Eq. (A4) at τ = 15 ms (upper dashed exponent) and τ = 30 ms (lower dashed exponent), and plotted by dotted curve according to the close-to-equilibrium-point (monoexponential) approach of Sokirko et al. (1994)

and the equilibrium volume reduction is:

$$\Delta V_0 = (\pi/1024) \cdot \varepsilon_0^2 \cdot \varepsilon_w^2 \cdot \left\{1 + a \cdot \lambda_m/(\lambda_{ex} \cdot d)\right\}^2 \cdot E^4 \cdot a^9 / \kappa^2 \tag{10}$$

Note that the rate of volume change due to vesicle deformation is the same as the deformation rate and is much smaller than the rate of membrane electroporation caused by Maxwell-Wagner interfacial polarization with the characteristic time constant $\tau_m = a \cdot C_m \cdot (\lambda_{in}^{-1} + 0.5 \cdot \lambda_0^{-1})$ = 0.43 μs, where C_m = 10 mF m^{-2} is the specific membrane capacitance and λ_{in} = 0.1 S m^{-1} is the conductivity of electrolyte in the vesicle interior (Neumann 1989). As the characteristic electroporation time is ≤0.5 μs for sea urchin eggs (Hibino et al. 1993) and ≤1.7 μs for lipid vesicles (Kakorin et al. 1996), membrane electroporation precedes the electrodeformation due to volume reduction (characteristic time constant ≈15 ms at E = 1 MV m^{-1}). Therefore, the vesicle deformation and thus the increase in salt concentration in the extravesicular medium are rate controlled by electrolyte flow from the vesicle interior through the membrane pores of constant surface area.

From Eq. (9) it is seen that the vesicle deformation rate decreases with the vesicle radius as steeply as $1/a^9$ (!). The decrease with increasing field strength follows a $1/E^2$ = dependence. For comparison, if the deformation is close to the equilibrium ($F_d \approx F_c$), it relaxes monoexponentially as is familiar for small deviations from equilibrium. If the entire deformation kinetics are approximated by only one exponential, τ^{-1} would be inversely proportional to a^{10} E^4 (Sokirko et al. 1994). In our experimental case this close-to-equilibrium approximation is inadequate. Our two-exponential "fork approximation" is apparently more satisfactory (Fig. 5) to analyze the deformation kinetics of small vesicles.

If Eq. (7) and Eq. (8) are applied to the analysis of $\Delta\lambda^I(t_E)/\lambda_0$ (Fig. 2a), we obtain the characteristic volume relaxation time τ = 15 ± 2 ms, the bending rigidity κ = (4.1 ± 0.3) · 10^{-20} J, and the fraction of porated membrane surface $f_p = (N \cdot \pi\, r_p^2)/(4 \cdot \pi \cdot a^2)$ = 0.0025 (0.25 ± 0.03%), resulting in a maximum of N = 39 ± 3 pores of mean pore

radius $r_p = 0.85 \pm 0.05$ nm per vesicle, at the field strength $E = 1$ MV m^{-1} and at a pulse duration of $t_E < 55 \pm 5$ ms. For comparison, the radius of so-called stable secondary pores (20 s after pulsing), induced in erythrocyte membranes by an exponential field pulse of $E_0 = 0.7$ MV m^{-1} and a decay time constant of $\tau_E = 40$ μs was estimated to be 0.75 ± 0.5 nm (Deuticke and Schwister 1989). The increase in the pore fraction of the erythrocyte membrane with increasing field strength was suggested to be due to an increase in pore density rather than in the pore radius. In our range $0.5 \le E/(\text{MV m}^{-1}) \le 1.0$ and $t_E \le 55 \pm 5$ ms the pore density and thus f_p are constant, because the transmembrane conductivity increase should prevent a further increase in the pore density (Kakorin et al. 1996). The characteristic volume relaxation time constant τ increases with the square of the field strength (Eq. (9)). For example, at $E = 0.5$ MV m^{-1} we obtain $\tau \approx 4$ ms, whereas at $E = 1.0$ MV m^{-1}, $\tau \approx 16$ ms. Then in the pulse duration range $30 \le t_E/\text{ms} \le 60$ and at $0.5 \le E/(\text{MV m}^{-1}) \le 1.0$, the relaxation of the vesicle deformation would last beyond the termination of the pulse. Thus $\Delta\lambda^I(t_E)/\lambda_0$ would reach a saturation value before vesicle electroaggregation and electrofusion begin (Fig. 3a). The analysis of the field dependencies of the $\Delta\lambda^I(E)/\lambda_0$ in the range $30 \le t_E/\text{ms} \le 60$ with Eq. (7) and Eq. (8) not only yields the same bending rigidity $\kappa = (4.1 \pm 0.3) \cdot 10^{-20}$ J, but also suggests that neither the rigidity of the membrane nor the mean vesicle radius change in the time interval $0 \le t_E/\text{ms} \le 60$ at $E \le 1$ MV m^{-1}.

The steep increase in $\Delta\lambda^I(t_E)/\lambda_0$ after the plateau region (Fig. 2a) is suggested to be due to electroaggregation and electrofusion of vesicles. Consistent with the turbidity data, the electroaggregation and partial electrofusion of vesicles, leads to an increase in the effective vesicle size. This, in turn, increases transiently the transmembrane field and thus the extent and the rate of the electroporation (Neumann 1989). As the pore number N and mean pore radius r_p increase, the characteristic volume relaxation τ decreases ($\tau < 15$ ms). Therefore the values of $\Delta\lambda^I(E)/\lambda_0$ at $t_E > 60$ ms (Fig. 3b) may be analyzed with Eq. (8) in the limit of $\Delta V \approx \Delta V_0$. So far as ΔV_0 does not depend either on N, or on r_p (Eq. (10)), only the bending rigidity κ and the vesicle mean radius are adjustable parameters of the analysis of the field dependencies of $\Delta\lambda^I(E)/\lambda_0$ (Fig. 3b) with Eq. (7) and Eq. (8). At $E = 1$ MV m^{-1} and $a = 50$ nm the analysis yields the bending rigidity $\kappa/J = 3.1$, 1.6 and $1.5 \pm 0.3 \cdot 10^{-20}$ at the pulse durations $t_E/\text{ms} = 65$, 70, 75, respectively. However, the fraction of membrane porated area can hardly be larger than 0.2% (Hibino et al. 1993), thus the bending rigidity κ should remain constant even on vesicle electroaggregation and electrofusion. The more adequate analysis of the same data in Fig. 3(b), but now under the assumption of constant $\kappa = 4.1 \cdot 10^{-20}$ J, gives the mean vesicle radii $a/\text{nm} = 55$, 65, 68 ± 5 at the pulse durations $t_E/\text{ms} = 65$, 70, 75, respectively. Accordingly, the steep increase in the dependencies $\Delta\lambda^I(E)/\lambda_0$ (Fig. 3b) is mainly due to the increase in the mean vesicle radius from $a = 50$ to 75 nm after vesicle electroaggregation and electrofusion.

Conductivity phase II

The conductivity phase II ($\Delta\lambda^{II}(t_E)/\lambda_0$) is consistently analyzed as diffusion of salt ions through the annealing pores after the termination of the field pulse. Applying Fick's first law and assuming a monoexponential resealing of the pore area with the rate coefficient k_R (Eq. (A9), the molar amount of electrolyte n^{in} in the vesicle interior is given by (see Appendix):

$$\frac{n^{in}(t)}{n_0^{in}} = \exp\left(-\left(k_f^0 / k_R\right) \cdot \left(1 - e^{-k_R \cdot t}\right)\right) \tag{11}$$

where n_0^{in} is the amount of electrolyte in the vesicle inside at the end of the pulse and k_f^0 is the efflux coefficient given by:

$$k_f^0 = \frac{P_p \cdot S_p^0}{V^{in}} = \frac{3 \cdot P_p \cdot f_p^0}{a} \tag{12}$$

where $f_p^0 = N \cdot r_p^2/(4 \cdot a^2)$ is the fraction of the porated area at the end t_E of the electric pulse, $S_p^0 = N^0 \cdot \pi \cdot r^2$ is the maximum total area of pore surfaces, $P_p = \gamma_p \cdot D/d$ is the pore permeability coefficient, D is the diffusion coefficient of the ions passing through the electropores, and γ_p is the pore partition coefficient, given by $\gamma_p = [n^p]/[n^{in}]$, where $[n^p]$ and $[n^{in}]$ are the concentrations of ions in the pore water and within the vesicle, respectively. According to Kohlrausch's first law for diluted solutions, Eq. (11) can be rewritten as (see Appendix):

$$\frac{\Delta\lambda^{II}(t)}{\lambda_0} \approx \frac{\Delta\lambda^{II}}{\lambda_0} \cdot \left(1 - e^{-k_R t}\right) \tag{13}$$

where $\Delta\lambda^{II}/\lambda_0$ is the amplitude value of the phase II at $t \to \infty$. Hence the efflux coefficient can be expressed as (see Appendix):

$$k_f^0 \approx k_R \cdot \Delta\lambda^{II}/\lambda_{max} \tag{14}$$

The coefficients k_f^0 and k_R were determined by analysis of the conductivity relaxations (Fig. 1c) and the field dependencies of the conductivity amplitude (Fig. 3c) with Eq. (13) and Eq. (14). The pore resealing coefficient k_R does not depend on the pulse duration or on the field strength in the ranges $t_E = 10$ to 100 ms and $E = 0.5$ to 1.0 MV m^{-1}, respectively (as expected for resealing without field). Experimentally, we find $k_R = 0.10 \pm 0.02$ s^{-1}. Since k_R is a constant, the initial pore size and pore structure should not be dependent on t_E and E. Similarly, Deuticke and Schwister (1989) suggested that the pore creation-resealing cycle in erythrocytes is determined to a major extent by increasing and decreasing the pore density, while the pore radius remains practically constant, rationalizing the fact the resealing rate of the pores after the field pulse does not alter with t_E and E.

The efflux coefficient k_f^0 of the electroporated vesicles, $\Delta\lambda^{II}(t_E)/\lambda_0$ (Fig. 2b) and $\Delta\lambda^{II}(E)/\lambda_0$ (Fig. 3c), however, depends on the pulse duration and field strength, respectively (Fig. 6a, b). Equation (12) yields numerical values

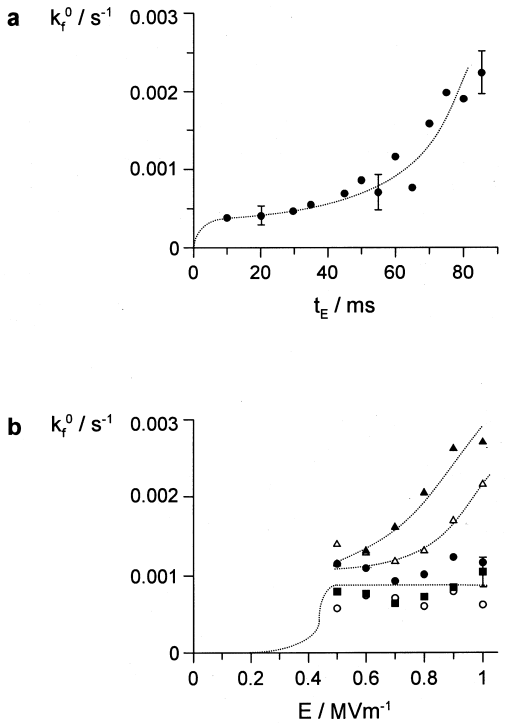

Fig. 6 Efflux rate coefficient k_f^0 as a function of **a** pulse duration t_E at E = 1.0 MV m^{-1}, **b** field strength E at t_E/ms = 30 (○), 50 (●), 65 (■), 70 (△), 75 (▲). The rate coefficient of pore resealing $k_R = 0.10 \pm 0.02$ s^{-1} is found to be independent on t_E and E. Experimental conditions as in Fig. 1

for the pore permeability coefficient of NaCl ions in the pores: $P_{p,NaCl} = k_f^0 \cdot a/(3 \cdot f_p^0)$. In the range $0.5 \le$ MV m^{-1} ≤ 1 and for $t_E = 50$ ms we obtain $k_f^0 = (8 \pm 2) \cdot 10^{-4}$ s^{-1} (Fig. 6b) and $f_p^0 = (2.5 \pm 0.3) \cdot 10^{-3}$; hence $P_{p,NaCl} = (5.6 \pm 0.5) \cdot 10^{-9}$ m s^{-1}. Note, the conventional membrane permeability coefficient P_m refers to the total membrane surface area and not solely to the area of passage sites. Thus, $P_{m,NaCl} = P_{p,NaCl} \cdot f_p = 1.4 \cdot 10^{-11}$ m s^{-1}. One is inclined to compare this $P_{m,NaCl}$ value with that of, for instance, the so-called 'postulated' pores of the erythrocyte membrane (20 s after an exponentially decaying field of initial strength $E_0 \le 0.7$ MV m^{-1} with time constant of 40 μs): $P_{m,K^+} \le 4.72 \cdot 10^{-9}$ m s^{-1} (Deuticke and Schwister 1989). The value P_{m,K^+} (erythrocyte) is about 100-fold larger than $P_{m,NaCl}$ (lipid vesicle). However, the red blood cells are a factor ≈50 larger than our vesicles. Therefore, at the same external field, the transmembrane voltage and thus the extent of electroporation are correspondingly higher.

If one takes the diffusion coefficient of NaCl in the pores to be equal to that in the free solution $D \approx 2 \cdot 10^{-9}$ m^2 s^{-1} at 273 K, the pore partition coefficient (γ_p) for NaCl ions in the membrane pore and bulk solution is $\gamma_p = P_p \cdot d/D \approx 1.4 \cdot 10^{-8}$. The conventional membrane partition coefficient γ_m, which refers to the total membrane surface, is than given by: $\gamma_m = \gamma_p \cdot f_p \approx 0.35 \cdot 10^{-10}$. Indeed, γ_m is rather small, but the value is physically reasonable for the penetration of ions into the dielectric medium of the lipid membrane.

Electroaggregation and electrofusion of vesicles

The increase in $\Delta OD/OD_0$ reflects increasing turbidity and is too large to originate from vesicle deformation alone. Most likely vesicle electroaggregation and electrofusion are responsible for the large turbidity increase. Electromicrographs of pulsed vesicles indeed show larger aggregates, appearing to be parallel with increasing $\Delta OD/OD_0$ (data not shown). Theoretically, the Rayleigh-Debye approximation (Wyatt 1973) for coated spheres and spheroids shows that the turbidity is proportional to the product of $n \cdot V^2$, where n is the number of particles per unit volume, $V = (4/3) \cdot \pi \cdot a^3$ is the mean particle volume and a is the radius of equivalent sphere. Therefore, an increase in the mean equivalent radius of aggregates or fusionates could lead to an increase in OD, even if n decreases with time.

The electric field-induced Maxwell stress increases with a^2 (Eq. (A2)). At given external field the electric potential drop $|\Delta\varphi| \approx 1.5 \cdot E \cdot a$ across the vesicle membrane increases linearly with a. The larger the size of the vesicle aggregates or fusionates, the larger are the extent and rate of membrane electroporation and vesicle deformation at a given field. Electroaggregation, followed probably by electrofusion, therefore leads to a larger electroporated membrane area and to further vesicle deformation. Consequently, there is additional leakage of electrolyte from the vesicle interior rationalizing the steep increase in $\Delta\lambda^I(t_E)/\lambda_0$ (E = 1 MV m^{-1}, Fig. 2a) as well as in $\Delta\lambda^I(E)/\lambda_0$ (Fig. 3) at $t_E > 55 \pm 5$ ms. The increase in the fraction f_p of porated membrane area alone results in a less pronounced increase in the after-field diffusion phase II, $\Delta\lambda^{II}(t_E)/\lambda_0$ and $\Delta\lambda^{II}(E)/\lambda_0$, at E = 1 MV m^{-1} and $t_E > 55 \pm 5$ ms (Fig. 2b and Fig. 3c, respectively).

Theoretically, an estimate for the time constant τ_{app} of approach, resulting in contact of two spherical vesicles in an electric field, is given by (see Appendix):

$$\tau_{app} \approx \frac{\eta \cdot \left(\gamma_o \left(\gamma_o \left(\gamma_o^2 \left(\frac{1}{5}\gamma_o + \frac{3}{8} \right) - \frac{1}{2} \right) - \frac{15}{4} \right) - 7\frac{9}{10} \right)}{8 \cdot u^2 \cdot \varepsilon_o \cdot \varepsilon_w \cdot E^2} \quad (15)$$

where $\gamma_0 = h_0/a$ is the average reduced distance and h_0 is the average distance between the vesicle centers at E = 0, respectively. If $\gamma_0 \ge 10$, the error in the use of Eq. (15) is less than 4.5%. The parameter u (Eq. (A16)) contains the total conductivity of vesicles λ_{ves} and the conductivity of medium λ_{ex} (Eq. (A17)). At the vesicle concentration [Ves] = $7.5 \cdot 10^{12}$ mL^{-1}, we obtain $\gamma_0 = 10$. Substitution of the time $t_E = 55 \pm 5$ ms from Fig. 2 and Fig. 6(a) in Eq. (15) finally yields $u = -0.27 \pm 0.03$, negative because of $\lambda_{ves} < \lambda_{ex}$. At E = 1 MV m^{-1}, $t_E = 55$ ms we find with Eq. (A17) that $\lambda_{ex} = 0.63$ mS m^{-1} (Fig. 2a). Substitution of the values of λ_{ex} and u in Eq. (A17) yields the total vesicle conductivity:

$$\lambda_{ves} = \lambda_{ex} \frac{1 + 2 \cdot u}{1 - u} = 0.23 \pm 0.02 \text{ mS m}^{-1} \quad (16)$$

Equation (16) shows that the total vesicle conductivity is 37% of the λ_{ex}. For comparison, the u-parameter for red

cell ghosts in 20-mM sodium phosphate buffer of conductivity 260 mS m^{-1} is u = –0.42, which corresponds to a total conductivity of the cells of λ_{cel} = 29 mS m^{-1}, that is approximately 11% of the surrounding electrolyte (Foster and Sowers 1995).

Since the non-electroporated lipid membrane is practically an electrical insulator, the total conductivity of the vesicles is predominantly due to electropores. If the electropores are filled with the electrolyte of conductivity λ_{in} from the vesicle interior, then the total conductivity of the vesicles λ_{ves} can be estimated with help of the fraction f_p of the electroporated area by:

$$\lambda_{ves} = f_p \cdot \lambda_{in} \tag{17}$$

Substitution of Eq. (17) in Eq. (16) yields for the fraction of porated membrane area:

$$f_p = \frac{\lambda_{ex}}{\lambda_{in}} \cdot \frac{1+2\cdot u}{1-u} \tag{18}$$

Insertion of u = –0.27, λ_{ex} = 0.63 mS m^{-1} and λ_{in} = 0.1 S m^{-1} in Eq. (18) yields $f_p = (2.3 \pm 0.3) \cdot 10^{-3}$, which is small but expected for the maintenance of interfacial polarization despite a few conductive pores. In the field direction the total resistance of a vesicle (Fig. 1 a) is the sum of the resistances (R_m) of the two pole cap membranes and the vesicle interior (R_{in}). Since $R_m \gg R_{in}$, we obtain $\lambda_{ves} \approx a/(R_m \cdot S)$. Because the membrane conductivity is $\lambda_m \approx d/(R_m \cdot S)$, substitution yields: $\lambda_m = \lambda_{ves} \cdot d/a = 23 \pm 2\ \mu S\ m^{-1}$.

Discussion

The most interesting experimental finding is the plateau in the dependence of $\Delta\lambda^I(t_E)/\lambda_0$ on the pulse duration t_E (Fig. 2 a). In addition to the electrodeformation of vesicles, another mechanism underlying the plateau may be considered. If no vesicle deformation occurs, the intravesicular electrolyte remains mainly in the vesicle interior for the short time of the pulse. If there were a significant electrodiffusion of ions through the pores, there would be no plateau in $\Delta\lambda^I(t_E)/\lambda_0$. The plateau in the first phase $\Delta\lambda^I(t_E)/\lambda_0$ could be due to a step-like increase in the membrane conductivity caused by electropores. The fraction of porated membrane area could level off because of an increase in the transmembrane conductivity λ_m up to the saturation value or because of a decrease of the transmembrane voltage (Kakorin et al. 1996). However, estimates show that even an infinite increase in the transmembrane conductivity λ_m and thus in the total conductivity of vesicles λ_{ves} can not describe the large amplitude value of $\Delta\lambda^I(t_E)/\lambda_0$. Actually, the maximum relative increase in the conductivity of the suspension of perfectly conductive electroporated vesicles is given by:

$$\Delta\lambda/\lambda_0 = \left(K_m^{cond} - K_m^{nonc}\right)/K_m^{nonc}, \tag{19}$$

where the ratio $K_m^{nonc} = \lambda_0/\lambda_s$ of the conductivity λ_0 of a suspension of non-conductive particles to that λ_s of pure solution (continuous phase) is given by (Meredith and Tobias 1962):

$$K_m^{nonc} = 8 \cdot (2 - f) \cdot (1 - f)/((4 + f) \cdot (4 - f)) \tag{20}$$

where f is the volume fraction of the dispersed phase (particles). The analogous ratio K_m^{cond} for the suspension of perfectly conductive electroporated vesicles in water is given by:

$$K_m^{cond} = (1 + f) \cdot (2 + f)/((1 - f) \cdot (2 - f)) \tag{21}$$

If the volume fraction of vesicles in our experiment is $f = 2.8 \cdot 10^{-3}$ (±3%), Eq. (19) yields $\Delta\lambda/\lambda_0 = 0.013$, which is about four times smaller than the experimental value corresponding to the plateau in $\Delta\lambda^I/\lambda_0 \approx 0.05$ at E = 1 MV m^{-1} (Fig. 2 a). Therefore, the membrane electroporation alone cannot explain the conductivity increase in the first phase. A significant efflux of electrolyte from vesicle interior due to deformation is required to describe this large increase in suspension conductivity.

We note that f_p = 0.23 ± 0.03%, obtained with Eq. (18) is close to the fraction of porated area (f_p = 0.25 ± 0.03%) estimated with Eq. (8). Thus, the independent determination of f_p from the characteristic vesicle deformation time τ and from the time constant τ_{app} of vesicle approach in an electric field yields the same value. If vesicle precipitation on the electrodes contributed to the kinetics of $\Delta\lambda^I(t_E)/\lambda_0$, $\Delta\lambda^{II}(t_E)/\lambda_0$ and $\Delta OD(t_E)$, the pore fraction f_p obtained at $t_E \approx 15$ and $t_E \approx 55$ ms should be very different. It thus appears that the sequence of events starting with membrane electroporation followed by slower vesicle elongation, finally leading to electroaggregation and electrofusion, is an adequate quantitative description of the conductometric and turbidimetric data.

In the range $0 \le E/(MVm^{-1}) \le 0.5$ the values of $\Delta\lambda^I(E)/\lambda_0$ and $\Delta\lambda^{II}(E)/\lambda_0$ are very small and lie within the margin of error. Therefore, E = 0.5 MVm^{-1} is an apparent threshold for Na^+ and Cl^- ion flow through the membrane pores. Although there is no threshold field strength associated with the lipid rearrangements of ME, the secondary processes such as ion transport exhibit thresholds. Here, the maximum value of the threshold transmembrane potential drop for the vesicle radius a = 50 nm is $\Delta\varphi_{th} = -1.5 \cdot a \cdot E = -37.5$ mV (Neumann 1989). The value is about ten times smaller than that reported for cells treated with millisecond electric pulses (Weaver 1995). Surprisingly, the high vesicle curvature $H = 1/a = 2.0 \cdot 10^7\ m^{-1}$ and the hydrostatic pressure in the vesicle interior $p \ge 26\ Nm^{-2}$ induced by an external field E ≥ 0.5 MV m^{-1} (pulse duration $t_E \ge 10$ ms) permit the electroporation of the lipid membrane and make it permeable to ions at the unusually low transmembrane potential drop of 37 mV. Note that Maxwell's hydrostatic pressure alone, without membrane electroporation, can not produce rupture of the membrane. Actually, the 50-nm (radius) unilamellar DOPG (dioleoyl phosphatidyl glycerol) vesicles do not rupture when they experience an osmotic gradient up to 0.5 osmol kg^{-1}, corresponding to the hydro-

static pressure of about 10^6 N m^{-2} (White et al. 1996). Probably the large electrolyte flow through the membrane can facilitate the membrane electroporation and bring about a formation of large crater-like pores (Neumann et al. 1992). The radius of most cells is usually 100-fold larger than a = 50 nm. Therefore, the area difference eleasticity (ADE) energy (Seifert and Lipowsky 1995; Seifert 1996) of cells is much smaller than that of small vesicles such that it can not be converted to pore formation free energy (Neumann and Kakorin 1996; Tönsing et al. 1997). Therefore, a cell membrane of low curvature requires a larger voltage to be electroporated than the highly curved membrane of *small* vesicles. This finding should open new horizons in the optimization of electroporation techniques and its application in the electroporative delivery of chemotherapeutica to tumor cells.

In conclusion, the conductivity and turbidity data of the salt filled vesicles in an electric field can be quantitatively rationalized as a sequence of rapid membrane electroporation, followed by slower vesicle deformation due to volume reduction by efflux, electroaggregation and vesicle electrofusion. For small vesicles, neither membrane superstructure nor thermal membrane undulations are required to describe the kinetics of the field-induced conductivity and turbidity changes in terms of membrane electroporation and vesicle deformation.

Acknowledgements We thank the Deutsche Forschungsgemeinschaft for a grant Ne 227/9-2 to E. Neumann and the Deutscher Akademischer Austauschdienst for a stipend to S. Kakorin.

Appendix

The Hagen-Poisseuille transport relationship

The permeation of water through the lipid bilayer is the rate limiting factor for the deformation of the vesicle sphere. The volume flow from the vesicle interior to the bulk solution through N pores of mean radius r_p may be described by the Hagen-Poisseuille formula:

$$\frac{d\Delta V}{dt} = \frac{\pi \cdot r_p^4 \cdot N \cdot \Delta p}{8 \cdot d \cdot \eta} \tag{A1}$$

where $\Delta p = (F_d - F_c)/(4\pi a^2)$ is the surplus pressure in the vesicle interior, d is the membrane thickness, η is the viscosity of water in pores ($\eta \approx 10.02 \cdot 10^{-4}$ kg m^{-1}s^{-1} at 293 K). The amplitude of the generalized force F_d of the Maxwell stress for a DC field and conducting membrane is given by:

$$F_d = dE_d / d\zeta = (3\pi/5)\varepsilon_0 \cdot \varepsilon_w \cdot \{1 + a \cdot \lambda_m /(\lambda_{ex} \cdot d)\} \cdot E^2 \cdot a^2, \tag{A2}$$

where $\varepsilon_0 = 8.85 \cdot 10^{-12}$ J^{-1}C^2 m^{-1} is the vacuum permittivity, ε_w the dielectric constant of water (ε_w = 78 at 293 K), λ_m the membrane conductivity, λ_{ex} the conductivity of the external medium and E_d the electrical energy of deformation (Winterhalter and Helfrich 1988).

The amplitude of the curvature-elastic generalized force (F_c), which acts in opposition to F_d, increases with the vesicle deformation according to:

$$F_c = dE_c/d\zeta = (96\pi/5) \cdot \kappa \cdot \zeta/a^2, \tag{A3}$$

where κ is the bending rigidity and E_c is the curvature-elastic energy of the ellipsoidal deformation (Winterhalter and Helfrich 1988). Note that, at stationarity, the two forces F_d and F_c become equal.

The explicit analytical solution of Eq. (A1) can be found in terms of the LambertW special function (Kakorin and Neumann, results not shown). However, if $F_d \gg F_c$ as is the case in the initial phase of the deformation, Eq. (A1) simplifies to:

$$\frac{d\Delta V}{dt} \approx \frac{\left(F_d^2 - F_c^2\right) \cdot N \cdot r_p^4}{32 \cdot d \cdot \eta \cdot F_d \cdot a^2} \tag{A4}$$

Equation (A4) can be solved in a more practical form than the LambertW function. The rate of the volume change analyzed with Eq. (A4) is about twice as large as the rate calculated with the exact Eq. (A1). In the final phase of vesicle deformation characterized by $F_d \approx F_c$, however, the difference $(F_d^2 - F_c^2)$ in Eq. (A4) is very close to zero and Eq. (A4) approaches the exact Eq. (A1) (Fig. 5). The analysis of the kinetics of the volume change with Eq. (A4) leads to a maximum of 19% underestimation of the mean pore radius r_p.

Substitution of Eq. (A2) and Eq. (A3) in Eq. (A4) yields:

$$\frac{d\Delta V}{dt} \approx \upsilon - \tau^{-1} \cdot \Delta V \tag{A5}$$

where $\upsilon = (3\pi/160) \cdot \varepsilon_0 \cdot \varepsilon_w \cdot \{1 + a \cdot \lambda_m/(\lambda_{ex} \cdot d)\} \cdot E^2 \cdot N \cdot r_p^4/(d \cdot \eta)$ and τ^{-1} is given by Eq. (9) in the text.

Integration of Eq. (A5) yields Eq. (8) where $\Delta V_0 = \upsilon \cdot \tau$ is given by Eq. (10).

For comparison, at DC fields and assuming a non-conductive unstretchable vesicle membrane as well as an only small ellipsoidal deformation of the vesicles ($\zeta \ll a$) and zero spontaneous curvature, the equilibrium value ζ_0 corresponding to the balance of Maxwell stress and curvature-elastic forces is given by (Winterhalter and Helfrich 1988):

$$\zeta_0 = (1/32) \cdot \varepsilon_0 \cdot \varepsilon_w \cdot \{1 + a \cdot \lambda_m /(\lambda_{ex} \cdot d)\} \cdot E^2 \cdot a^4 / \kappa \tag{A6}$$

Substitution of Eq. (A6) in Eq. (5) of the text yields the equilibrium volume reduction as in Eq. (10).

Fick's transport relationship

According to Fick's first law, the mole efflow expressed in the terms of changes in the amount of electrolyte n^{out} in the extravesicular medium or that of the vesicle interior n^{in} is proportional to the molar salt concentration gradient in

the direction x across the membrane of thickness d between x = 0 and x = d:

$$\left(\frac{\partial n^{out}}{\partial t}\right)_x = -\left(\frac{\partial n^{in}}{\partial t}\right)_x = P_d \cdot S_p \cdot \left(\frac{n^{out}}{V^{out}} - \frac{n^{in}}{V^{in}}\right) \quad \text{(A7)}$$

where $S_p = N \cdot \pi \cdot r^2$ is the total area of pores in membrane, P_p is the pore permeability coefficient, V^{in} and V^{out} are the volume of extra- and intravesicular media, respectively. Note that the conventional permeability coefficient, referring to the total membrane surface, is $P_m = f_p \cdot P_p$.

Under the experimental conditions $n^{in} \gg n^{out}$ and $V^{in} \ll V^{out}$, corresponding to our experimental case, the concentration gradient is well approximated by:

$$\left(\frac{n^{out}}{V^{out}} - \frac{n^{in}}{V^{in}}\right) \approx -\frac{n^{in}}{V^{in}} \quad \text{(A8)}$$

In the simplest case, pore resealing is modeled by one closing process according to:

$$S_p(t) = S_p^0 \cdot e^{-k_R \cdot t} \quad \text{(A9)}$$

where S_p^0 is the maximum total pore surface area at the end of the electric pulse and k_R is the rate coefficient of pore resealing.

Substitution of Eq. (A8) and Eq. (A9) in Eq. (A7) and integration yield Eq. (11) of the text.

Kohlrausch's first law of the independent migration of ions

According to the Kohlrausch's first law for diluted solutions we have $\Delta\lambda^{II}(t) = F \cdot (v_{Na} + v_{Cl}) \cdot \Delta n^{out}(t)/V^{out} = -F \cdot (v_{Na} + v_{Cl}) \cdot \Delta n^{in}/V^{out}$, where F is the Faraday constant and v_{Na}, v_{Cl} are the mobilities of the Na^+ and Cl^- ions, respectively. Hence, Eq. (11) of the text can be rewritten as:

$$\frac{\Delta\lambda^{II}(t)}{\lambda_0} = \frac{\Delta\lambda^{II}_{max}}{\lambda_0}\left(1 - \exp\left(-\left(k_f^0 / k_R\right) \cdot (1 - e^{-k_R \cdot t})\right)\right) \quad \text{(A10)}$$

where $\Delta\lambda^{II}_{max} = \lambda_{max} - \Delta\lambda^{I} = F \cdot (v_{Na} + v_{Cl}) \cdot n_0^{in}/V^{out}$.

The relative amplitude (at $t \to \infty$) of the phase II $\Delta\lambda^{II}/\lambda_0$ is given by:

$$\frac{\Delta\lambda^{II}}{\lambda_0} = \frac{\Delta\lambda^{II}_{max}}{\lambda_0}\left(1 - \exp\left(-k_f^0 / k_R\right)\right) \quad \text{(A11)}$$

Since the measured values are: $\Delta\lambda^{II}/\lambda_0 < 0.2$ (Fig. 3c) and $\Delta\lambda^{II}_{max}/\lambda_0 < 7.0$, under our experimental conditions the strong nonequality $k_f^0/k_R \ll 1$ holds, thus the exponents in Eq. (A10) and Eq. (A11) can be expanded in a series, respectively, in which the terms of higher order than a value proportional to (k_f^0/k_R) are negligibly small. Hence:

$$\frac{\Delta\lambda^{II}(t)}{\lambda_0} \approx \frac{\Delta\lambda^{II}_{max}}{\lambda_0} \cdot \left(k_f^0 / k_R\right) \cdot (1 - e^{-k_R t}) \quad \text{(A12)}$$

and:

$$\frac{\Delta\lambda^{II}}{\lambda_0} \approx \frac{\Delta\lambda^{II}_{max}}{\lambda_0} \cdot \left(k_f^0 / k_R\right) \quad \text{(A13)}$$

Rearrangement of Eq. (A13) yields the ratio:

$$k_f^0/k_R \approx \Delta\lambda^{II}/\Delta\lambda^{II}_{max} \quad \text{(A14)}$$

The substitution of Eq. (A14) in Eq. (A12) leads to the one-parameter (k_R) Eq. (13) for the description of the conductivity relaxation phase II.

At $E \leq 1$ MV m^{-1}, we obtain $\Delta\lambda^{I}/\lambda_{max} < 0.06$ (Fig. 3b). Therefore $\Delta\lambda^{II}_{max} \approx \lambda_{max}$ and the efflux coefficient can be expressed as in Eq. (14).

Approach of two spherical vesicles in an electric field

At low field intensities, the approach of two equal spherical vesicles in an electric field due to induced electrical dipole moments is given by (Foster and Sowers 1995):

$$\frac{d\gamma}{dt} = \frac{8 \cdot u^2 \cdot \varepsilon_o \cdot \varepsilon_w \cdot E^2 \cdot \Delta A(\gamma)}{\eta \cdot \gamma^4} \quad \text{(A15)}$$

where $\gamma = h/a$, h is the distance between the centers of two approaching vesicles. The parameter u for conductive media (λ_{ex}) and conductive vesicles (λ_{ves}) is given by:

$$u = \frac{\lambda_{ves} - \lambda_{ex}}{\lambda_{ves} + 2 \cdot \lambda_{ex}} \quad \text{(A16)}$$

Hence,

$$\lambda_{ex} = \lambda_0 + \Delta\lambda^{I}(t_E), \quad \text{(A17)}$$

where $\Delta\lambda^{I}$ corresponds to the plateau at $t_E \leq 55 \pm 5$ ms (Fig. 2a).

The function $\Delta A(\gamma)$ characterizing the hydrodynamic interaction of the vesicles is given by (Batchelor 1976):

$$\Delta A(\gamma) = 1 - \frac{3}{2\gamma} + \frac{1}{\gamma^3} - \frac{15}{4\gamma^4} + O(\gamma^{-6}), \quad \text{(A18)}$$

Insertion of Eq. (A18) in Eq. (A15) and integration yields Eq. (15) for the estimate of the time constant τ_{app} of approach of vesicles resulting in contact.

References

Batchelor GK (1976) Brownian diffusion of particles with hydrodynamic interaction. J Fluid Mech 74:1–29

Deuticke B, Schwister K (1989) Leaks induced by electrical breakdown in the erythrocyte membrane. In: Neumann E, Sowers AE, Jordan C (eds) Electroporation and electrofusion in cell biology. Plenum Press, New York, pp 127–148

Foster KR, Sowers AE (1995) Dielectrophoretic forces and potentials induced on pairs of cells in an electric field. Biophys J 69:777–784

Heller R, Jaroszeski MJ, Glass LF, Messina JL, Rapaport DP, Deconti RC, Fenske NA, Gilbert RA, Mir LM, Reintgen DS (1996) Phase I/II Trial for the treatment of cutaneous and subcutaneous tumors using electrochemotherapy. Cancer 77:964–971

Helfrich W, Servuss RM (1984) Undulations, steric interaction and cohesion of fluid membranes. Nuovo Cimento 3D:137–151

Hibino M, Itoh H, Kinosita K (1993) Time courses of cell electroporation as revealed by submicrosecond imaging of transmembrane potential. Biophys J 64:1789–1800

Hope MJ, Bally MB, Webb G, Cullis PR (1985) Production of large unilamellar vesicles by rapid extrusion procedure. Characterization of size distribution, trapped volume and ability to maintain a membrane potential. Biochim Biophys Acta 812:55–65

Hyuga H, Kinosita K, Wakabayashi N (1993) Steady-state deformation of a vesicle in alternating electric-fields. Bioelectrochem Bioenergetic 32:15–25

Kakorin S, Stoylov SP, Neumann E (1996) Electro-optics of membrane electroporation in diphenylhexatriene-doped lipid bilayer vesicles. Biophys Chem 1996, 58:109–116

Kinosita KJr, Hibino M, Itoh H, Shigemori M, Hirano K, Kirino Y, Hayakawa T (1992) Events of membrane electroporation visualized on time scale from microsecond to seconds. In: Chang DC, Chassy BM, Saunders JA, Sowers AE (eds) Guide to electroporation and electrofusion. Academic Press, New York, pp 29–46

Klösgen B, Helfrich W (1993) Special features of phosphatidylcholine vesicles as seen in cryo-transmission electron-microscopy. Eur Biophys J 22:329–340

Kummrow M, Helfrich W (1991) Deformation of giant lipid vesicles by electric-fields. Phys Rev A 44:8356–8360

MacDonald RC, MacDonald RI, Menco BPM, Takeshita K, Subbarao NK, Hu L (1991) Small-volume extrusion apparatus for preparation of large, unilamellar vesicles. Biochim Biophys Acta 1061:297–303

Mayer LD, Hope MJ, Cullis PR (1986) Vesicles of variable size produced by rapid extrusion procedure. Biochim Biophys Acta 885:161–168

Meredith RE, Tobias CW (1962) II. Conduction in heterogeneous systems. Adv Electrochem Electrochem Eng 2:15–47

Neumann E (1989) The relaxation hysteresis of membrane electroporation. In: Neumann E, Sowers AE, Jordan C (eds) Electroporation and electrofusion in cell biology. Plenum Press, New York, pp 61–82

Neumann E, Werner E, Sprafke A, Krüger K (1992) Electroporation phenomena – electrooptics of plasmid DNA and of lipid bilayer vesicles. In: Jennings BR, Stoylov SP (eds) Colloid and molecular electrooptics. IOP, Bristol, UK, pp 197–206

Neumann E, Kakorin S (1996) Electrooptics of membrane electroporation and vesicle shape deformation. Curr Opin Colloid Interface Sci 1:790–799

Seifert U (1995) The concept of effective tension for fluctuating vesicles. U Physic B Cond Matt 97:299–309

Seifert U, Lipowsky R (1995) Morphology of Vesicles: In: Lipowsky R, Sackmann E (eds) Structure and dynamics of membranes, 1A. Elsevier North-Holland, pp 403–463

Seifert U (1996) Morphology and dynamics of vesicles. Current Opinion in Coll Int Sci 1:350–357

Sokirko A, Pastushenko V, Svetina, Zeks B (1994) Deformation of lipid vesicle in an electric field: a theoretical study. Bioelectrochem Bioenerg 34:101–107

Steiner U, Adam G (1984) Interfacial properties of hydrophilic surfaces of phospholipid films as determined by method of contact angles. Cell Biophysics 6:279–299

Tönsing K, Kakorin S, Neumann E, Liemann S, Huber R (1997) Annexin V and vesicle membrane electroporation. Eur Biophys J 26:307–318

Weaver JC (1995) Electroporation in cells and tissues – A biophysical phenomenon due to electromagnetic-fields. Radio Sci 30:205–221

White G, Pencer J, Nickel BG, Wood JM, Hallett FR (1996) Optical changes in unilamellar vesicles experiencing osmotic stress. Biophys J 71:2701–2715

Winterhalter M, Helfrich W (1988) Deformation of spherical vesicles by electric fields. J Coll Int Sci 122:583–586

Wyatt PJ (1973) Differential light scattering techniques. Methods Microbiol 8:183–263